journal of the mechanical behavior of biomedical materials 126 (2022) 104969

Contents lists available at ScienceDirect

Journal of the Mechanical Behavior of Biomedical Materials

journal homepage: www.elsevier.com/locate/jmbbm

Research paper

An study on the influence of collagen fiber directions in TAVs performance using FEM

S. Suárez [a], J.A. López-Campos [a,b,*], A. Segade [a,b], C.G. Veiga [c], V.A. Jiménez [d]

[a] CINTECX, Departamento de Ingeniería Mecánica, Universidade de Vigo, Vigo, Spain
[b] Biomechanics Research Group, Galicia Sur Health Research Institute (IIS Galicia Sur), SERGAS-UVIGO, Vigo, Spain
[c] Cardiology Research Group, Galicia Sur Health Research Institute (IIS Galicia Sur), SERGAS-UVIGO, Vigo, Spain
[d] Cardiology Department, Complexo Hospitalario Universitario de Vigo (CHUVI), Vigo, Spain

ARTICLE INFO

Keywords:
TAV
Aortic valve
Anisotropy
Hyperelasticity
Tissue constitutive modeling

ABSTRACT

Transcatheter Aortic Valve Implantation (TAVI) or Replacement (TAVR) is a promising treatment for aortic valve stenosis, consisting of a procedure to replace a damaged native aortic valve by a bioprosthetic one. This replacement valve control the flow of blood using leaflets that are similar to the ones of a native aortic valve. Commonly manufactured using bovine or porcine pericardium, it is a tissue histologically composed of collagen fibers embedded into a nearly-isotropic matrix, where their distribution makes the pericardium behave as an anisotropic hyperelastic material. Because of such complicated behavior, bioprosthetic pericardium valves are, as expected, sensitive to the distribution and orientation of these fibers in such device.

Therefore, the objective of this work is a thorough systematic study on the influence of these fibers' distribution. First, a Finite Element model of a bioprosthetic valve is generated; then, a material routine to accurately describe the behavior of pericardium is implemented in a commercial software package; in addition, a dedicated algorithm to specify the direction of fibers is developed. Finally, a systematic study on the influence that fiber orientations have on the overall behavior of the TAV is performed.

As a result of this study, two extreme behaviors are highlighted depending on the preferential orientation of collagen fibers; namely, one with fibers in circumferential direction and the opposite with fibers in an axial orientation. Then, it is concluded that the behavior of fibers in circumferential direction is very sensitive to small variations of the orientation angle, whereas such orientation is not as determining when the aim is to achieve a behavior near to the one corresponding with axial orientation.

1. Introduction

The aortic valve is a native valve located at the root of the aorta, which connects this vessel with the left ventricle. Its three leaflets, thin and flexible membranes, are the main structures guaranteeing unidirectional flow (Ho, 2009) between the ventricle and the aorta by opening during the ventricular systole and preventing blood backflow into the heart during the rest of cardiac cycle by keeping closed.

Over time, the valve leaflets become stiffer and thicker, which could lead to cardiac diseases and ultimately produce aortic stenosis (Sahasakul et al., 1988). A common treatment is the Transcatheter Aortic Valve Implantation or TAVI (Brewer et al., 1977). During such intervention, a bioprosthetic heart valve called Transcatheter Aortic Valve (TAV) is implanted inside the native degenerated aortic valve by a minimally invasive procedure, consisting of introducing the TAV through a catheter and expanding it when reaching its final position where it remains fixed, replacing the native one.

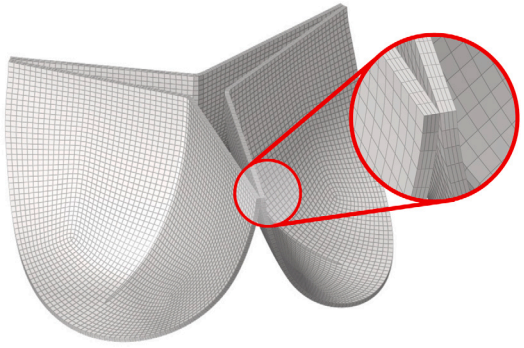

Fig. 1. 3D mesh of the leaflets.

* Corresponding author at: CINTECX, Departamento de Ingeniería Mecánica, Universidade de Vigo, Vigo, Spain.
E-mail address: joseangellopezcampos@uvigo.es (J.A. López-Campos).

https://doi.org/10.1016/j.jmbbm.2021.104969
Received 6 September 2021; Received in revised form 21 October 2021; Accepted 6 November 2021
Available online 20 November 2021

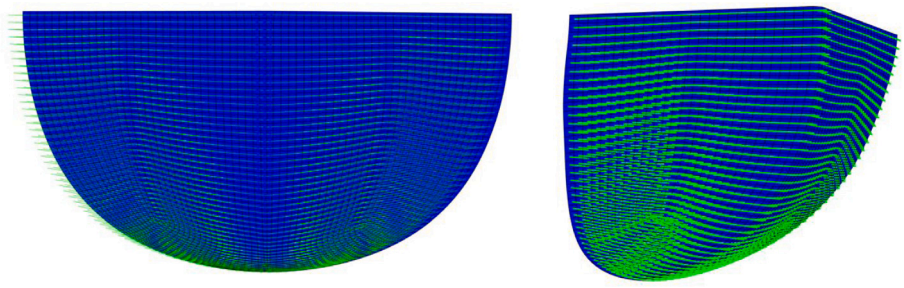

Fig. 2. Flat configuration (left) and conformed configuration (right) of a leaflet.

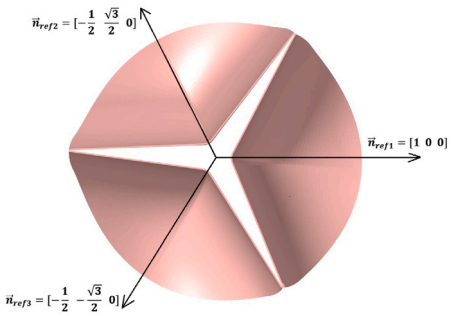

Fig. 3. Normals in the flat configuration for each leaflet.

$$cos\theta = \mathbf{n}_{flat} \cdot \mathbf{n}_{conformed}$$

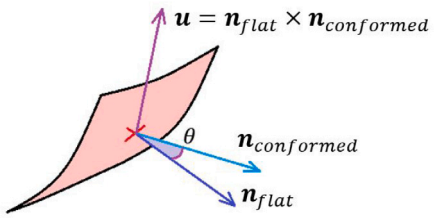

Fig. 4. Rotation of an element defined as an in-plane rotation.

Customarily made from the animal pericardium, the tissue of artificial leaflets in TAVs is histologically composed of a collagen network embedded within a continuous matrix, which is highly complex and consists of water, heavy proteins, and elastic fibers, exhibiting a nearly isotropic behavior. In contrast with the overall behavior of the pericardium, which is highly anisotropic because of the formation of long bundles in a preferred direction made by long collagen molecules.

Because of their role in valve performance, many experts have carried out significant efforts to simulate the mechanical behavior of leaflets using numerical methods (Sun et al., 2005; Kim et al., 2008; Sun et al., 2010). These numerical simulation tools allow reproducing and predicting the behavior of systems, but the accuracy of their results is highly dependent on the input data and models used to replicate the actual geometry, material, and boundary conditions.

In this sense, most of soft biological tissues are characterized by a complex, non-linear and anisotropic behavior (Fung et al., 1979; Holzapfel et al., 2000; Gasser et al., 2005; Cai et al., 2016; López-Campos et al., 2020); even though, some other authors also used isotropic hyperelastic models to simulate their behavior (Hart et al., 2004; Schiavone and Zao, 2015) and there are even authors who compare the accuracy of both types of material models (Joda et al., 2016). This work uses an anisotropic hyperelastic model (Travaglino et al., 2020) to reproduce the behavior of the TAV leaflets. The paper

Table 1
Parameters for the material constitutive model.

C_{10} [MPa]	C_{01} [−]	k_1 [MPa]	k_2 [−]	D [MPa^{-1}]
0.0186	7.935	0.0279	56.352	0.0001

focuses on the influence of the fiber preferred directions over the mechanical behavior of the TAV, from the definition of a Finite Element (FE) model to study such issue; hence, addressing both the anisotropic behavior and the direction of fibers, crucial features to consider when constructing the model.

Therefore, the paper outline is as follows: first, an introduction of the Finite Element Model of the TAV, followed by a description of the material model used to simulate the behavior of pericardium, and an explanation of the algorithm used to define the fiber orientation. Subsequently given is the performance of a systematic study focusing on the dependence of the TAV behavior on the fiber-preferred directions and its evaluation in terms of fiber stretch, the strain energy density in the matrix, and Effective Orifice Area (EOA), and finally, highlights of some of the conclusions obtained from the study.

2. Finite element model

The Finite Element Model of the valve leaflets was made using the commercial software package ABAQUS. Taking as starting point the geometry of the leaflets, a structured mesh was generated using 3-D elements (C3D8R and C3D6). A mesh sensibility analysis was carried out with two, four and six elements through the thickness for a particular orientation of collagen fibers. Since no meaningful changes were noticed with four and six elements, the model with four elements through the thickness was used, as shown in Fig. 1. Reduced integration of elements is selected to avoid volumetric locking (Coombs et al., 2018) since behavior of leaflets is expected to correspond to a nearly-incompressible material.

Since this study focuses on the leaflets' particular behavior, we had to define and reproduce the boundary conditions as closely and realistically as the actual operating conditions in the aorta. Therefore, we pinned the leaflets at the central node of their edge to allow for subsequent rotations and then applied pressure to the faces that were closest to the ventricle, which has a value defined as 10 mmHg. Such value was chosen according to Boron and Boulpaep (2009) and represents the maximum difference between blood pressure before and after the valve at the opening step.

2.1. Material model

Frequently, the material used to manufacture TAVs is bovine pericardium, a tissue of complex histology, essentially composed of a connective tissue matrix with a complex collagen network (Deutsch et al., 2019). This internal structure leads to hyperelastic behavior with significant anisotropy (Caballero et al., 2017).

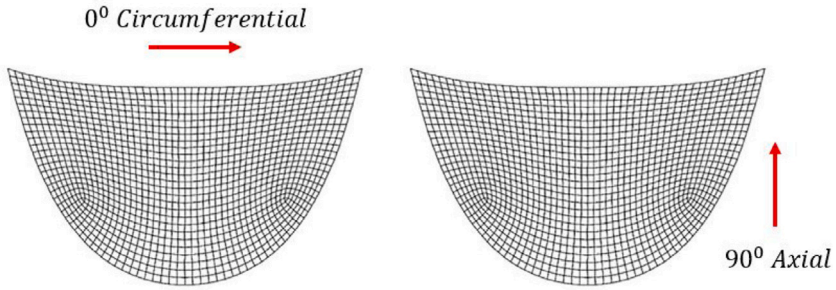

Fig. 5. Initial orientation of fiber in circumferential and axial directions.

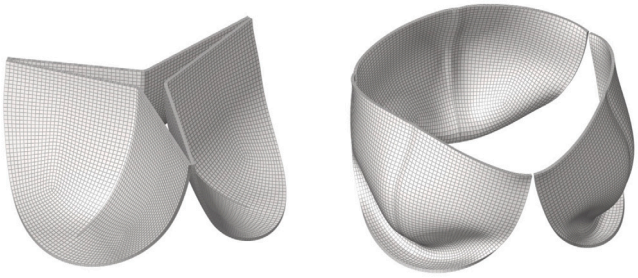

Fig. 6. Geometry of leaflets before (left) and after (right) the pressure is applied.

According to bibliography, a material is defined as hyperelastic when its mechanical behavior can be described by a strain energy function (SEF). The SEF states one relationship between the strain energy and a measure of deformation in terms of the right Cauchy Green deformation tensor (Holzapfel, 2000), defined as:

$$\mathbf{C} = \mathbf{F}^t \cdot \mathbf{F}, \qquad \mathbf{F} = \frac{\partial \mathbf{x}}{\partial \mathbf{X}}, \tag{1}$$

where tensor **F**, called deformation gradient, establishes a relationship between initial or undeformed configuration and actual or deformed configuration. Therefore, SEF is defined generally in terms of the tensor **C** invariants and a parameter set which depends on in the material. For this particular tissue, its behavior was modeled using the following function (Travaglino et al., 2020):

$$W(\mathbf{C}, \mathbf{a}_0) = C_{10}\left\{e^{C_{01}(\bar{I}_1-3)} - 1\right\} + \frac{k_1}{2k_2}\left\{e^{k_2(\bar{I}_4-1)^2} - 1\right\} + \frac{1}{D}(J-1)^2, \tag{2}$$

where $\bar{I}_1$ and $\bar{I}_4$ are invariants of tensor **C** (Spencer, 1971). Eq. (2) shows that the strain energy depends not only on tensor **C** but also on vector $\mathbf{a}_0$. This dependency is given through the definition of $\bar{I}_4$:

$$\bar{I}_1 = \mathbf{C} : \mathbf{I}; \qquad \bar{I}_4 = \mathbf{a}_0 \cdot \mathbf{C}\mathbf{a}_0 = \lambda^2 \tag{3}$$

In Eq. (3), $\mathbf{a}_0$ is a unit vector that defines the preferential direction of pericardium collagen fibers in each element and in the undeformed configuration. Consequently, the material model used to describe the behavior of pericardium can produce a direction-dependent behavior so that the model can reproduce the main features in the pericardium elastic response.

The particular material used for this analysis is bovine pericardium 0.32 mm thick (Murdock et al., 2018), and the constants used to model its behavior are summarized in Table 1:

This material model is implemented in ABAQUS using the UMAT routine. Further, the preferential directions of fibers in each element have to be transferred to ABAQUS for the definition of the fourth invariant ($\bar{I}_4$ in Eq. (3)), which is a procedure also done employing the UEXTERNALDB subroutine.

2.2. Definition of fiber directions in pericardium

A critical feature in defining the behavior of the pericardium is the preferred direction of the collagen fibers (Caballero et al., 2017; Sacks and Chuong, 1998). Using Eq. (2) a stiffer behavior in one specific direction is able to be simulated; however, the definition of $\mathbf{a}_0$ could be challenging in such a complex geometry as a leaflet is. To solve this problem, a dedicated algorithm is implemented in MATLAB to compute the preferential direction of fibers and to transfer such directions to ABAQUS through the UEXTERNALDB routine.

Based on the manufacturing process of the leaflets of a TAV, this algorithm takes as starting point a flat configuration with fibers oriented in one particular direction. Then, tissue is conformed to acquire the final shape of a leaflet; during this process, fibers adapt to the new shape of tissue, so, the direction of fibers at each point has to be modified to fit the new shape of the tissue, as detailed in the example shown in Fig. 2.

The left side of the picture corresponds to the flat configuration, where preferential direction of fibers is entirely horizontal. In picture, such direction is highlighted in green and represented by vectors $\mathbf{a}_0^{flat}$. Finally, the tissue is conformed, so the elements, initially in a plane configuration move to its final position. Consequently, the preferential directions overcome a rotation and vector $\mathbf{a}_0^{conformed}$ has to be computed for each single element.

To define the rotation of each element from the flat configuration to the conformed one, the following procedure was carried out for each one of the elements in the model. Such procedure is based on the change of the element orientation that is evaluated through the change happened on its normal.

Therefore, each element has a normal in flat configuration that is different depending on the specific leaflet as detailed in Fig. 3.

In addition when the tissue acquire the shape of a leaflet (conformed configuration) each element changes its orientation and then, the normal changes its direction. To evaluate such rotation we used a rotation matrix **R** that is build according to P.M. Rodrigues' definition for a rotation about an axis (Rodrigues, 1840), and for further clarity, it is as follows:

$$\mathbf{R} = \begin{bmatrix} cos\theta + u_x^2(1-cos\theta) & u_x u_y(1-cos\theta) - u_z sin\theta & u_x u_z(1-cos\theta) + u_y sin\theta \\ u_y u_x(1-cos\theta) + u_z sin\theta & cos\theta + u_y^2(1-cos\theta) & u_y u_z(1-cos\theta) - u_x sin\theta \\ u_z u_x(1-cos\theta) - u_y sin\theta & u_z u_y(1-cos\theta) + u_x sin\theta & cos\theta + u_z^2(1-cos\theta) \end{bmatrix} \tag{4}$$

where u_x, u_y and u_z are the components of a unit vector defining the direction of the rotation axis, while θ represents the rotation angle about such axis.

First, rotation axis is computed using the vector product between the normal vector in flat $\mathbf{n}_{flat}$ and conformed $\mathbf{n}_{conformed}$ (Fig. 4).

$$\mathbf{u} = \mathbf{n}_{flat} \times \mathbf{n}_{conformed} \tag{5}$$

Afterwards, the rotation angle can be easily computed using the dot product between the normal vectors in flat and in conformed

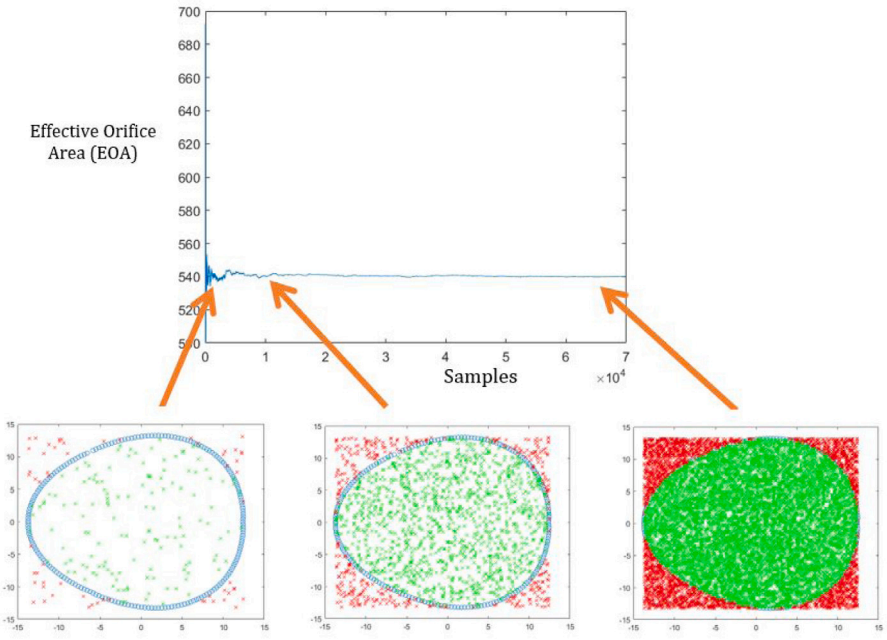

Fig. 7. Scheme of the algorithm to measure EOA using a Monte-Carlo method.

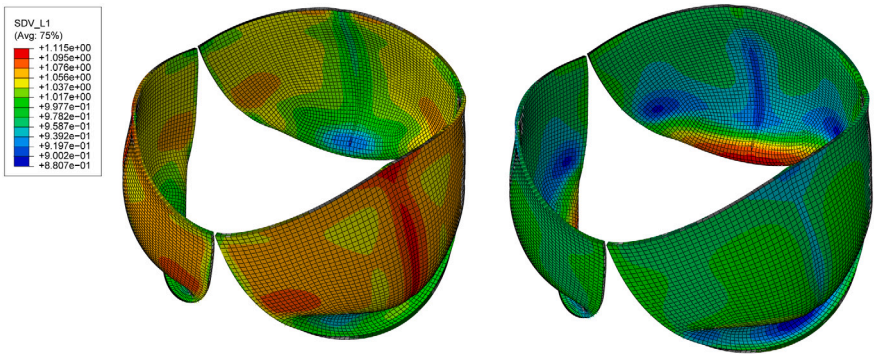

Fig. 8. Fiber stretch contours with fibers in circumferential (left) and axial (right) directions.

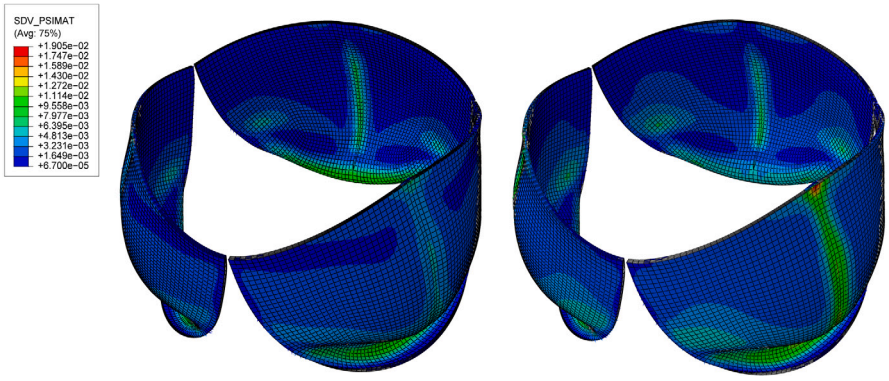

Fig. 9. Contours of strain energy in the matrix with fibers in circumferential (left) and axial (right) directions.

configuration since both are unit vectors. Finally, rotation matrix **R** is easily computed according to Eq. (4).

$$cos\theta = \mathbf{n}_{flat} \cdot \mathbf{n}_{conformed} \tag{6}$$

Once the rotation of the element is characterized through its rotation matrix, then the same rotation is applied to fiber directions. So, the same rotation matrix, and thus, we calculated the fiber preferential direction in each element by using the following equation:

$$\mathbf{a}_0^{conformed} = \mathbf{R} \cdot \mathbf{a}_0^{flat} \tag{7}$$

To conclude, preferential directions are written into a file and this information is transferred to ABAQUS using the aforementioned UEXTERNALDB routine.

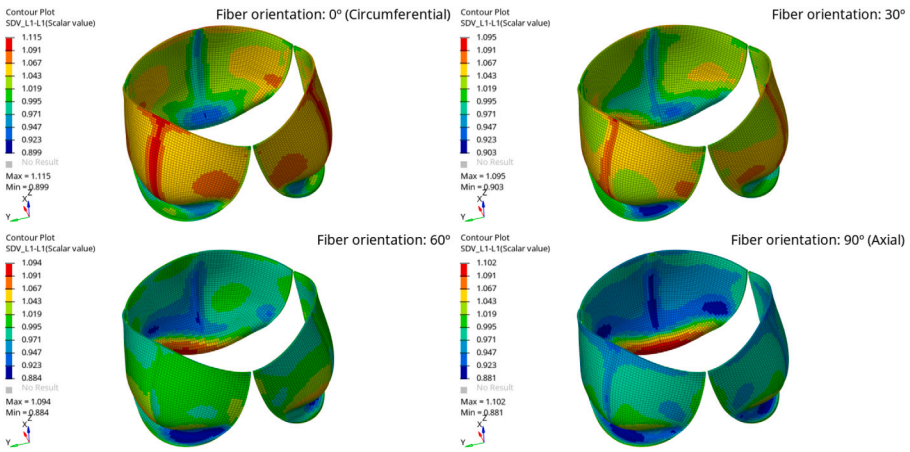

Fig. 10. Contours of fiber stretch in several fiber arrangements.

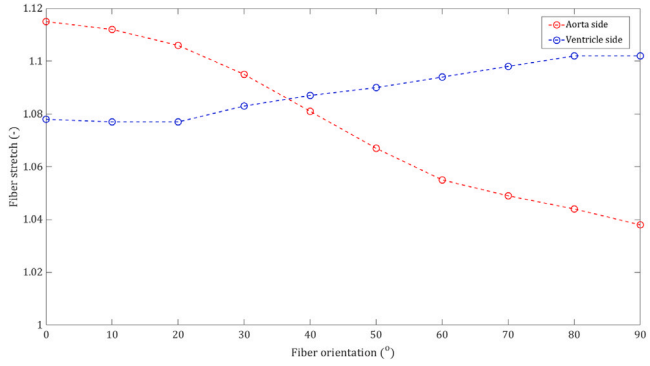

Fig. 11. Influence of orientation angle of the fibers in maximum fiber stretch.

3. Systematic study on fiber directions

The pericardium's inherent anisotropy caused by the collagen fibers dispersed over the matrix could lead to the different behavior of the TAV depending on the orientation of such fibers. Regarding this feature, we conducted a systematic study on fiber directions.

To perform this study, the fiber orientation in the reference flat configuration varies from 0° or circumferential direction to 90° or axial direction using a 10° step procedure (Fig. 5), performed in 10 simulated cases.

Fiber directions are then computed in conformed configuration for each case, according to the procedure detailed in Section 2.2. Such configuration is taken as starting point to start with the FE computation. A pressure on the leaflet's face is applied according to the boundary conditions defined in Section 2. In Fig. 6a comparison between the geometry of leaflets before and after the pressure is applied is shown.

Even though we used the same mesh and boundary conditions in all cases, fiber orientations transferred to ABAQUS through the routine UEXTERNALDB were different for each one.

Afterwards, we compared the structural behaviors of the leaflets regarding maximum fiber stretch (λ in Eq. (3)), maximum strain energy in the matrix, and Effective Orifice Area (EOA).

Since the shape EOA is complex and irregular, we used a Monte-Carlo method (Siswantoro et al., 2014) to measure the EOA in its final deformed configuration, by computing random sample points which are generated inside one rectangle of a known area. Then, the algorithm determined which sampling points lie inside the TAV area when the valve opened. Finally, we computed EOA using the ratio between the points lying inside the area and the total number of samples, as shown in Fig. 7. In order to guarantee the convergence of Monte-Carlo simulations, the algorithm stopped generating sample points when the error was below 0.25%.

4. Results

This section shows, first, the study of two opposite fiber orientations, circumferential and axial; therefore, fiber stretch, as well as matrix strain energy contours, are analyzed in both configurations. Then, the evolution of results from circumferential to axial orientation is shown with more details, accounting from intermediate orientation of fibers.

4.1. Comparison between the circumferential and axial fiber orientation

Fig. 8 shows the contours that exhibited fiber stretching; at left panel, the contours corresponds to the circumferential direction of the fibers while, at right, they corresponds to the axial direction. As expected, in circumferential arrangement, fiber stretch is higher since fiber orientation tends to be towards the direction of maximum stress. This fact might also imply a stiffer behavior of the leaflet caused by the fibers strength.

Maximum fiber stretch occurred at the center the leaflets for circumferential orientation of the collagen bundles, reaching a value of 1.115. At that location, fiber stretch decreased as the fibers become oriented axially, up to values around 0.947 for axial orientation. So, the influence of fiber elasticity and strength is expected to be much more meaningful in configurations near to a circumferential arrangement of fibers.

Regarding to the matrix behavior, we evaluated the strain energy associated to the matrix, showing the contours in Fig. 9. At left, contour of the strain energy corresponding to a circumferential distribution of fibers is shown, while right panel corresponds with the results of the model where fibers are axially located.

The maximum value of the matrix strain energy appears at the center of leaflets as in the case of fiber stretch. Its value is $1.06 \cdot 10^{-2}$ mJ for fibers in circumferential direction, while in axial configuration, such value increases up to approximately $1.91 \cdot 10^{-2}$ mJ. In circumferential direction, fibers are mainly responsible for the structural stiffness of the leaflet. On the contrary, when their orientation is in axial direction, they do not stretch, and therefore, their role has to be covered by the extracellular matrix, which is a more flexible media than fibers.

4.2. Dependence on the fiber orientation

As we shown in the previous example, differences in the elasticity and relative importance of both components (fiber and matrix)

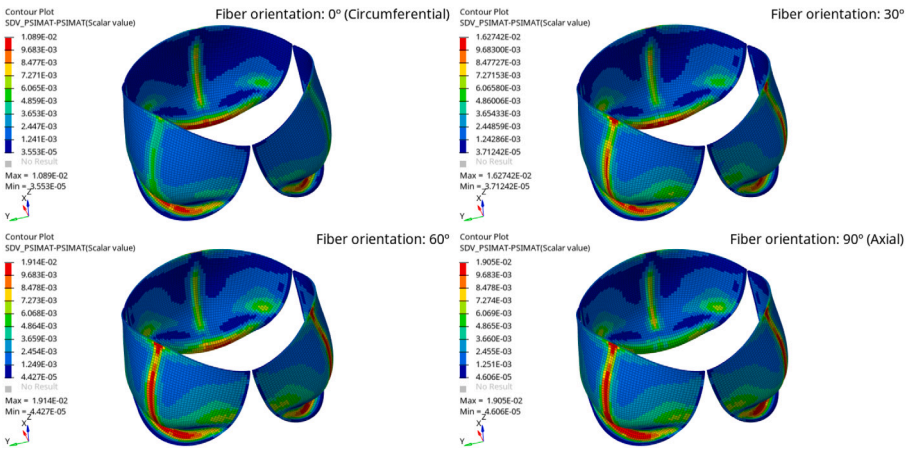

Fig. 12. Contours of matrix strain energy in several fiber arrangements.

determined a different mechanical behavior of the TAV in axial and circumferential configurations. In this section, our aim is to consider other possible fiber arrangements to find their influence on the system behavior.

In Fig. 10 several contours are shown. They represent the evolution of fiber stretch from circumferential to axial configuration. For an easy comparison, color scale is the same for all contours. As seen, zones where maximum stretch occurs differ depending on the orientation of fibers. In models near to circumferential configuration stretch is maximum at the center of leaflet and at the aorta side. Opposite, in models with an arrangement near to axial, the maximum stretch is located at the ventricle side of the leaflet and near to the base of the leaflet.

To account from these changes on the location of maximum values in Fig. 11 we show the maximum stretch value of the fibers for the leaflets at the aorta side and at the ventricle side as a function of the orientation angle of the fibers.

According to such results, maximum stretch of fibers is substantially influenced by the orientation angle of the collagen bundles, specially at the aorta side, while the influence at ventricle side is not as important. Therefore, in general, fiber elongation decreased as they leaning towards the axial direction of the fibers. So, fiber contribution to the stiffness of the leaflet is less important in configurations near to axial arrangement of fibers.

On the other hand, the influence of matrix is also measured using its maximum strain energy. As in the case of stretch, Fig. 12 represent the SEF in different models with different fiber orientations. Opposite to fiber stretch, SEF field is more uniform, so maximum values are located in similar locations in all models. However, as fibers become axially oriented SEF increases because matrix has to assume more structural function at the center of leaflets.

Regarding to the evolution of matrix strain energy, such magnitude linearly increases with angle up to 40°, when it started to lean to stabilization, as it is shown in Fig. 13. We could explain this fact through the evolution of fiber stretch aforementioned. Note the fact that, when the stretch of fibers is close to unit (60°), strain energy in matrix reaches an stable value.

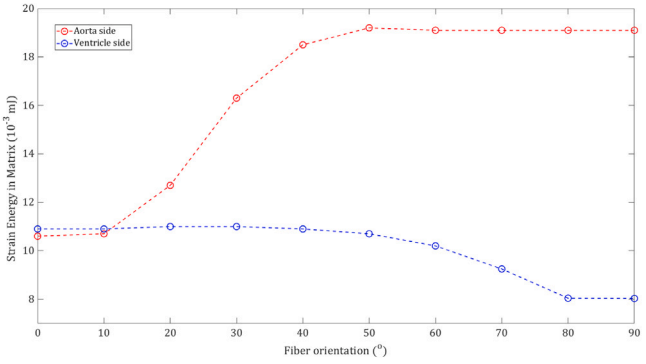

Fig. 13. Influence of angle fibers orientation in maximum strain energy density of the matrix.

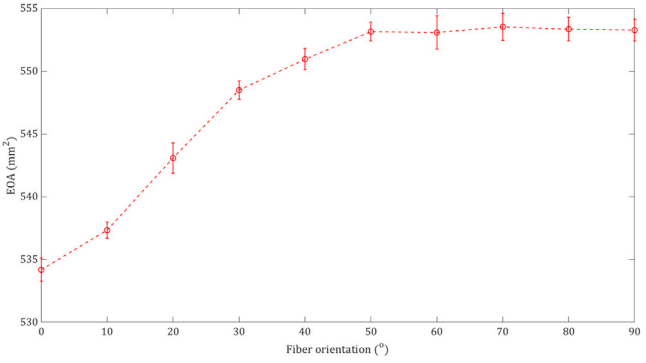

Fig. 14. Influence of angle fibers orientation in the Effective Orifice Area (EOA).

4.3. EOA (Effective Oriffice Area)

Because of the EOA measurement, it was observed that a minimum area of 534.18 mm^2 was reachable when the direction of the fibers was circumferential. A rapid increase of the area appeared up to 30°, and then, it began to increase more gradually until stabilization from 50° at a value of approximately 553 mm^2 (see Fig. 14).

The nature of the isotropic matrix makes it a more flexible material than the collagen fibers that suffer from a fast stiffening when stretched, meaning that, for the circumferential direction, in which the fibers' stretch was maximum, their behavior made the overall system stiffer.

However, in the absence of the collagen fibers' action, the rise in the material's flexibility implied higher deformation in the matrix, which led to a further increase in the EOA. Fig. 14 shows how the magnitude of the EOA varied regarding the angle's orientation since the higher it is, the higher the deformation energy density of the matrix, with stabilization starting at 50°, indicating that its magnitude does not vary despite the increase in the direction angle of the fibers until reaching the axial direction.

5. Conclusions

This study focused on the influence of collagen fiber directions in the behavior of the leaflets of a TAV. The results obtained demonstrate that as the orientation of fiber is near to axial, the whole system becomes more flexible because of the decrease in stiffness caused by the reduction in the stretch of the collagen fibers. This fact occurs because fibers act as stiffeners of the tissue when they are oriented towards the direction of efforts.

The systematic study shows that the mechanical behavior of the leaflets began to stabilize from 50° resulting in a practically constant EOA, caused by the contribution decrease of fibers in the overall system's behavior. From there, the matrix contribution became much more significant, being this isotropic matrix, a continuous element, the sole support of the effect of the external pressure.

To sum up, the collagen fibers orientation influences the mechanical response of the material during the opening of the valves up to an angle of 50°. Beyond this angle, the material's behavior does not alter because of slight variations in fiber orientation, being equivalent to a material with fibers oriented in the axial direction. Therefore, the accuracy in the orientation of fibers has to be especially guaranteed when a behavior near to a circumferential model is desirable, where fibers help to reinforce the tissue.

CRediT authorship contribution statement

S. Suárez: Conception and design of study, Analysis of data, Drafting the manuscript. **J.A. López-Campos:** Conception and design of study, Analysis of data, Drafting the manuscript. **A. Segade:** Supervision and revision of the manuscript, Funding acquisition. **C.G. Veiga:** Supervision and revision of the manuscript, Conceptualization. **V.A. Jiménez:** Supervision and revision of the manuscript, Conceptualization.

Declaration of competing interest

The authors declare that they have no known competing financial interests or personal relationships that could have appeared to influence the work reported in this paper.

Acknowledgment

This work was partially supported by the research project PGC2018-096696-B-I00 (Ministerio de Ciencia, Innovación y Universidades, Spain).

References

Boron, W.F., Boulpaep, E.L., 2009. Medical Physiology: A Cellular and Molecular Approaoch. Elsevier.

Brewer, R.J., M, Jr., R.M., Deck, J.D., Ritter, R.C., Trefil, J.S., Nolan, S.P., 1977. An in vivo study of the dimensional changes of the aortic valve leaflets during the cardiac cycle. J. Thorac. Cardiovasc. Surg. 74, 645–650. http://dx.doi.org/10.1016/s0022-5223(19)40896-9.

Caballero, A., Sulejmani, F., Martin, C., Pham, T., Sun, W., 2017. Evaluation of transcatheter heart valve biomaterials: Biomechanical characterization of bovine and porcine pericardium. J. Mech. Behav. Bimed. Mater. 75, 486–494. http://dx.doi.org/10.1016/j.jmbbm.2017.08.013.

Cai, R., Holweck, F., Feng, Z.-Q., Peyraut, F., 2016. A new hyperelastic model for anisotropic hyperelastic materials with one fiber family. Int. J. Solids Struct. 84, 1–16. http://dx.doi.org/10.1016/j.ijsolstr.2015.11.008.

Coombs, W.M., Charlton, T.J., Cortis, M., Augarde, C.E., 2018. Overcoming volumetric locking in material point methods. Comput. Methods Appl. Mech. Engrg. 333, 1–21. http://dx.doi.org/10.1016/j.cma.2018.01.010.

Deutsch, O., Bruehl, F., Cleuziou, J., Prinzing, A., Schlitter, A.M., Krane, M., Lange, R., 2019. Histological examination of explanted tissue-engineered bovine pericardium following heart valve repair. Interact. CardioVasc. Thorac. Surg. 30, 64–73. http://dx.doi.org/10.1093/icvts/ivz234.

Fung, Y.C., Fronek, K., Patitucci, P., 1979. Pseudoelasticity of arteries and the choice of its mathematical expression. Am. J. Physiol. 237 (5), 620–631. http://dx.doi.org/10.1152/ajpheart.1979.237.5.H620.

Gasser, T.C., Ogden, R.W., Holzapfel, G.A., 2005. Hyperelastic modelling of arterial layers with distributed collagen fibre orientations. J. R. Soc. Interface 3, 15–35. http://dx.doi.org/10.1098/rsif.2005.0073.

Hart, J.D., Peters, G.W.M., Schreurs, P.J.G., Baaijens, F.P.T., 2004. Collagen fibers reduce stresses and stabilize motion of aortic valve leaflets during systole. J. Biomech. 37 (3), 303–311. http://dx.doi.org/10.1016/s0021-9290(03)00293-8.

Ho, S.Y., 2009. Structure and anatomy of the aortic root. Eur. J. Echocardiogr. 10, i3–i10. http://dx.doi.org/10.1093/ejechocard/jen243.

Holzapfel, G.A., 2000. Nonlinear Solid Mechanics: A Continuum Approach for Engineering. Wiley.

Holzapfel, G.A., Gasser, T.C., Ogden, R.W., 2000. A new constitutive framework for arterial wall mechanics and a comparative study of material models. J. Elasticity Phys. Sci. Solids 61, 1–48. http://dx.doi.org/10.1023/A:1010835316564.

Joda, A., Jin, Z., Haverich, A., Summers, J., Korossis, S., 2016. Multiphysics simulation of the effect of leaflet thickness inhomogeneity and material anisotropy on the stress–strain distribution on the aortic valve. J. Biomech. 49 (12), 2502–2512. http://dx.doi.org/10.1016/j.jbiomech.2016.02.041.

Kim, H., Lu, J., Sacks, M.S., Chandran, K.B., 2008. Dynamic simulation of bioprosthetic heart valves using a stress resultant shell model. Ann. Biomed. Eng. 36 (2), 262–275. http://dx.doi.org/10.1007/s10439-007-9409-4.

López-Campos, J.A., Ferreira, J.P.S., Segade, A., Fernández, J.R., Natal, R.M., 2020. Characterization of hyperelastic and damage behavior of tendons. Comput. Methods Biomech. Biomed. Eng. 23 (6), 213–223. http://dx.doi.org/10.1080/10255842.2019.1710742.

Murdock, K., Martin, C., Sun, W., 2018. Characterization of mechanical properties of pericardium tissue using planar biaxial tension and flexural deformation. J. Mech. Behav. Biomed. Mater. 77, 148–156. http://dx.doi.org/10.1016/j.jmbbm.2017.08.039.

Rodrigues, P.M., 1840. Des lois géométriques qui régissent les déplacements d'un système solide dans l'espace, et de la variation des coordonnées provenant de ces déplacements considérés indépendamment des causes qui peuvent les produire. J. Math. Pures Appl. 5, 380–440.

Sacks, M.S., Chuong, C.J., 1998. Orthotropic mechanical properties of chemically treated bovine pericardium. Ann. Biomed. Eng. 26 (5), 892–902. http://dx.doi.org/10.1114/1.135.

Sahasakul, Y., Edwards, W.D., Naessens, J.M., Tajik, A.J., 1988. Age-related changes in aortic and mitral valve thickness: implications for two-dimensional echocardiography based on an autopsy study of 200 normal human hearts. Am. J. Cardiogr. 62, 424–430. http://dx.doi.org/10.1016/0002-9149(88)90971-x.

Schiavone, A., Zao, L.G., 2015. A study of balloon type, system constraint and artery constitutive model used in finite element simulation of stent deployment. Mech. Adv. Mater. Modern Process 1, http://dx.doi.org/10.1186/s40759-014-0002-x.

Siswantoro, J., Prabuwono, A.S., Abdullah, A., 2014. Volume measurement algorithm for food product with irregular shape using computer vision based on Monte Carlo method. J. ICT Res. Appl. 8, 1–17. http://dx.doi.org/10.5614/itbj.ict.res.appl.2014.8.1.1.

Spencer, A.J.M., 1971. Continuum Physics. Academic Press.

Sun, W., Abad, A., Sacks, M.S., 2005. Simulated bioprosthetic heart valve deformation under quasi-static loading. J. Biomech. Eng. 127 (6), 905–914. http://dx.doi.org/10.1115/1.2049337.

Sun, W., Li, K., Sirois, E., 2010. Simulated elliptical bioprosthetic valve deformation: Implications for asymmetric transcatheter valve deployment. J. Biomech. 43 (16), 3085–3090. http://dx.doi.org/10.1016/j.jbiomech.2010.08.010.

Travaglino, S., Murdock, K., Tran, A., Martin, C., Liang, L., Wang, Y., Sun, W., 2020. Computational optimization study of transcatheter aortic valve leaflet design using porcine and bovine leaflets. J. Biomech. Eng. 142, 1–8. http://dx.doi.org/10.1115/1.4044244.